Accelerated ^{19}F biomolecular magic-angle spinning NMR with paramagnetic dopants

Lea M. Becker[1], Giorgia Toscano[1,2], Anna Kapitonova[1], Rajkumar Singh[1], Undina Guillerm[1], Roman Lichtenecker[2], and Paul Schanda[1]

[1]Institute of Science and Technology Austria, Am Campus 1, 3400 Klosterneuburg, Austria
[2]Institute of Organic Chemistry, University of Vienna, Währinger Str. 38, 1090 Vienna, Austria

Correspondence: Paul Schanda (paul.schanda@ist.ac.at)

Abstract. The advantageous characteristics attributed to the ^{19}F nucleus have made it a popular target for NMR once again in recent years. Aside from solution NMR, an increasing number of studies have been conducted applying solid-state magic-angle-spinning NMR to fluorine-labeled samples. Here, the high chemical shift anisotropy and strong dipolar couplings can be utilized to get structural insights into proteins and measure long distances. Despite increasing popularity and promising benefits,

5 the sensitivity of biomolecular ^{19}F MAS NMR often suffers from slow longitudinal T_1 relaxation and therefore long recycle delays. In this work, we expand paramagnetic doping, an approach commonly used to reduce proton T_1 relaxation times, to ^{19}F-labeled biological samples. We study the effect of Gd(DTPA) and Gd(DTPA-BMA) on ^{19}F and ^{13}C T_1 and T_2 relaxation in a [5-^{19}F^{13}C]-tryptophan-labeled protein via ^{19}F-detected MAS NMR experiments. The observed paramagnetic relaxation enhancement substantially reduces measurement times of ^{19}F MAS NMR experiments without compromising resolution.

10 Additionally, we report the chemical-shift assignments of all four fluorotryptophan signals in the $12 \times 39\,\mathrm{kDa}$ large protein using a mutagenesis approach.

1 Introduction

Biomolecular ^{19}F nuclear magnetic resonance (NMR) has regained attention in recent years due to the unique properties of the ^{19}F nucleus and the diverse labeling strategies for proteins and nucleic acids which make it a versatile tool for a wide

15 range of applications and systems (Sengupta (2024); Gronenborn (2022); Juen et al. (2024); Overbeck et al. (2020); Heller et al. (2024)). Recently, there have been exciting developments in the synthesis of compounds for ^{19}F-labeling of proteins (Boeszoermenyi et al. (2019); Toscano et al. (2024a, b); Suleiman et al. (2024)): The introduction of a carbon-13 to form a ^{19}F$-^{13}$C spin pair facilitates new spectroscopic possibilities such as two-dimensional experiments and the exploration of the ^{19}F$-^{13}$C TROSY effect. Additional deuteration of labeling compounds can reduce the need for ^{1}H decoupling and lead to a

20 reduction of unwanted relaxation pathways.

In contrast to solution-state NMR, solid-state magic-angle-spinning (MAS) ^{19}F NMR was challenging for a long time due to the high chemical shift anisotropy (CSA) of the ^{19}F nucleus and strong dipolar ^{1}H$-^{19}$F couplings, which can lead to severe line broadening (Ulrich (2005)). Following the development of faster spinning and specialized probe designs that enable efficient

averaging and decoupling of the CSA and dipolar couplings, biomolecular ^{19}F MAS NMR is becoming more feasible. These

25 advancements have led to ^{19}F NMR studies of protein microcrystals, membrane proteins, and large biomolecular assemblies

such as virus capsides. The focus of these studies was set on assignments and structural investigations utilizing the possibility

to measure distances of up to 20 Å (Roos et al. (2018); Duan et al. (2022); Shcherbakov et al. (2019, 2021); Porat-Dahlerbruch

et al. (2022); Wang et al. (2018)).

Despite the large gyromagnetic ratio of the fluorine nucleus, the sensitivity of ^{19}F-excited MAS NMR experiments is often

30 limited by long longitudinal T_1 relaxation times, which are often several seconds (Duan et al. (2022); Roos et al. (2018); Wang

et al. (2018); Porat-Dahlerbruch et al. (2022)). As the recycle delay $\tau_{\text{r.d.}}$ for an optimal signal-to-noise ratio (SNR) is directly

related to the longitudinal relaxation of the excited nucleus ($\tau_{\text{r.d.}}^{\text{opt}} = 1.26 * T_1$; Schanda (2009)), most of the experiment time

is spent waiting for the spin polarization to build up again. The use of deuterated precursors for ^{19}F labeling results in even

longer T_1 relaxation, as short-range $^1\text{H}-^{19}\text{F}$ dipolar couplings are reduced and dipolar relaxation pathways are minimized.

35 Paramagnetic doping is an established and effective method to reduce the acquisition time of measurements. In solids, it has

primarily been used for experiments in which protons are the initially excited nuclei. The addition of a paramagnetic compound

to the sample, e.g., Cu^{2+} or Gd^{3+} chelates, results in enhanced nuclear spin relaxation. The longitudinal Γ^1 and transverse

Γ^2 paramagnetic relaxation enhancement (PRE) is given by (Solomon (1955); Bertini et al. (2001); Bloembergen and Morgan

(1961); Konig (1982))

40 $$\Gamma^1 \approx \frac{2}{15} \left(\frac{\mu_0}{4\pi}\right)^2 \frac{\gamma_{\text{I}}^2 g_{\text{e}}^2 \mu_{\text{B}}^2 S(S+1)}{r^6} \left(\frac{3\tau_{\text{c}}}{1+\omega_{\text{I}}^2\tau_{\text{c}}^2} + \frac{7\tau_{\text{c}}}{1+\omega_{\text{e}}^2\tau_{\text{c}}^2}\right)$$

$$\Gamma^2 \approx \frac{1}{15} \left(\frac{\mu_0}{4\pi}\right)^2 \frac{\gamma_{\text{I}}^2 g_{\text{e}}^2 \mu_{\text{B}}^2 S(S+1)}{r^6} \left(4\tau_{\text{c}} + \frac{3\tau_{\text{c}}}{1+\omega_{\text{I}}^2\tau_{\text{c}}^2} + \frac{13\tau_{\text{c}}}{1+\omega_{\text{e}}^2\tau_{\text{c}}^2}\right) \qquad (1)$$

with the vacuum permeability μ_0, the gyromagnetic ratio of the nucleus γ_{I}, the electron g-value g_{e}, the Bohr magneton μ_{B},

the electron spin quantum number S, the electron-nucleus distance r, the rotational correlation time τ_{c}, and the nuclear and

electron larmor frequencies ω_{I} and ω_{e}. The goal is to find a concentration of the paramagnetic compound in the buffer that,

45 on the one hand, significantly accelerates ^1H T_1 relaxation, allowing a shorter recycle delay and therefore faster acquisition,

and, on the other hand, does not shorten T_2, so as not to induce line broadening. While the paramagnetic effects depend on

the proximity of the unpaired electron, the enhancement of longitudinal relaxation is spread across the molecule from those

nuclei directly relaxed by the paramagnetic center to other nuclei via $^1\text{H}-^1\text{H}$ spin diffusion (Wickramasinghe et al. (2009)).

The first studies to achieve a significant increase in SNR per unit time utilized Cu^{2+}-EDTA as a dopant, which remains widely

50 used to date (Wickramasinghe et al. (2007, 2009)). However, the higher PRE effect of Gd^{3+} chelates, such as Gd(DOTA),

Gd(DTPA-BMA), or Gd(DTPA), enables the use of lower concentrations of the compound, reducing possible interactions with

the studied biomolecule and sample heating (Linser et al. (2007); Ullrich et al. (2014); Mroue et al. (2014); Öster et al. (2019)).

Even though paramagnetic doping was mainly applied for its effect on the T_1 relaxation of protons, it also increases the relax-

ation of other nuclei, with the strength of the effect being proportional to the squared gyromagnetic ratio of the nucleus (Eq. (1)).

55 Due to the high gyromagnetic ratio of ^{19}F, a significant reduction in measurement time can be expected for biomolecular ^{19}F

MAS NMR experiments with similar concentrations of paramagnetic compounds as are used for proton-excited experiments.

Transversal and longitudinal PREs of fluorine in solution were measured previously to obtain distance restraints between a fluorine atom and a paramagnetic moiety (Shi et al. (2012); Matei and Gronenborn (2016); Bondarenko et al. (2019); Huang et al. (2020)). In solids, Lu et al. demonstrated paramagnetic doping with Cu^{2+} ions in the context of fluorinated, crystalline pharmaceuticals for structural characterization by ^{19}F MAS NMR. They achieved a significant reduction of the ^{19}F T_1 relaxation times in their samples, resulting in approximately 2.5-times faster acquisition of fluorine NMR spectra, which highlights the potential benefits of combining paramagnetic doping and ^{19}F solid-state MAS NMR (Lu et al. (2020)).

In this work, we explore the potential benefits of paramagnetic doping for biomolecular ^{19}F MAS NMR on proteins, which has not been reported so far, to the best of our knowledge. Using the deuterated 5-fluorotryptophan-labeled protein TET2 ($12 \times 39\,kDa$), we measure ^{19}F and ^{13}C T_1 and T_2 as a function of the concentration of two Gd^{3+} complexes, Gd(DTPA-BMA) and Gd(DTPA). We find that a concentration of $8\,mM$ Gd(DTPA-BMA) is optimal to reduce measurement times of ^{19}F MAS NMR experiments through a decrease of the ^{19}F T_1 relaxation time without significant line broadening.

2 Methods

2.1 Protein production and purification

The aminopeptidase TET2 from *P. horikoshii* (UniProt entry O59196) was produced via overexpression of the pET41c-PhTET2 plasmid in *Escherichia coli* BL21(DE3) RIL cells. The plasmid is available from AddGene (https://www.addgene.org/182428/), which also comprises all plasmid details. For the resonance assignment, tryptophans were mutated into phenylalanines in different combinations either as single mutant (mutant 1: W106F), or as triple mutants (mutant 2 (only W106): W136F, W164F, W276F; mutant 3 (only W136): W106F, W164F, W276F; mutant 4 (only W164): W106F, W136F, W276F; mutant 5 (only W276): W106F, W136F, W164F). The ^{19}F labeling was either achieved with 5-fluoroindole (Sigma-Aldrich, catalogue number F9108) in protonated medium (mutants) or with $[5-^{13}C, 3, 4, 6-^2H_3]$-5-fluoroanthranilic acid (5FC-anthranilic acid) in deuterated medium (wild type).

The 5-fluoroanthranilic acid isotopologue was synthesized in-house by adapting the synthetic route reported by Suleiman et al. to the present labeling scheme; details of the synthesis will be published elsewhere.

The plasmid (kanamycin resistance) was transformed into competent BL21(DE3) RIL cells (chloramphenicol resistance) via heat shock. Unless otherwise mentioned, all cultures contained kanamycin and chloramphenicol, and shaking was performed at $200\,rpm$ and $37\,°C$.

5-fluoroindole labeling was achieved as follows. After precultures in LB medium and minimal M9 medium, the main culture was inoculated to an optical density at $600\,nm$ (OD_{600}) of 0.2 and shaken until it reached 0.6-0.7. At this point, $1\,g\,L^{-1}$ glyphosate (abcr, Karlsruhe, Germany; catalogue number AB505195) was added, and the culture was grown for $15\,min$ before $100\,mg\,L^{-1}$ 5-fluoroindole, $50\,mg\,L^{-1}$ L-tyrosine (Sigma T3754) and $50\,mg\,L^{-1}$ L-phenylalanine (Sigma 78019) was added. The culture was grown $45\,min$ and expression was induced with $1\,mM$ Isopropyl-β-D-thiogalactopyranosid (IPTG). Cells were harvested at $6500\,rcf$ for $15\,min$ after $4\,h$ of shaking.

Labeling with 5FC-anthranilic acid was achieved as follows. Cells were adjusted to deuterated M9 medium by growth in consecutive precultures of LB medium, and M9 medium prepared with 100% H_2O, 50% H_2O/50% D_2O, and 100% D_2O. The final preculture and the main culture were prepared with $^{15}NH_4Cl$ and D-$^2H_7$-glucose. The main culture was inoculated to an OD_{600} of 0.2 and shaken until it reached 0.6-0.7. At this point, $1\,g\,L^{-1}$ glyphosate, $50\,mg\,L^{-1}$ L-tyrosine, $50\,mg\,L^{-1}$ L-phenylalanine, and $15\,mg\,L^{-1}$ 5FC-anthranilic acid were added, and the culture was shaken for $40\,min$. The temperature was then reduced to $28\,°C$ for $15\,min$ before induction with $1\,mM$ IPTG. Cells were grown overnight at $28\,°C$ and then harvested at $6500\,rcf$ for $15\,min$.

The cell pellet was resuspended in lysis buffer ($50\,mM$ Tris-HCl pH 7.5, $150\,mM$ NaCl, $0.05\,mg\,mL^{-1}$ DNase, $2\,mM$ $MgCl_2$, $0.025\,mg\,mL^{-1}$ RNase and 0.5 tablets cOmplete EDTA-free protease inhibitor), kept on ice for $30\,min$, and sonicated for $2\,min$. A heat shock was performed at $80\,°C$ for $15\,min$. After addition of $10\,mL$ buffer A ($20\,mM$ Tris-HCl pH 7.5, $100\,mM$ NaCl), the cell debris was collected by centrifugation at $46000\,rcf$ for $40\,min$ at $4\,°C$. The supernatant was washed with buffer A using an Amicon ultra centrifugal filter with a molecular weight cutoff of $100\,kDa$ before loading onto a RE-SOURCE Q column (Cytiva) and eluted with a gradient over 10 column volumes from buffer A to buffer B ($20\,mM$ Tris-HCl pH 7.5, $1\,M$ NaCl). The fractions containing the protein were concentrated, loaded onto a HiLoad 10/300 Superdex 200 pg column (Cytiva), and eluted in buffer A.

2.2 Sample preparation

Samples for solid-state MAS NMR were prepared by batch crystallization of TET2 with 2-Methyl-2,4-pentanediol (MPD; Sigma 68340) (Gauto et al. (2019a)). A solution of $10\,mg\,mL^{-1}$ protein and the paramagnetic compound (where applicable) in buffer A was mixed with MPD in a v/v ratio of 1:1. The concentration given for the paramagnetic compound in the following is related to the final concentration in the sample, including MPD. The microcrystals were filled into a $1.3\,mM$ MAS rotor (Bruker) by ultracentrifugation overnight at $68000\,rcf$.

2.3 NMR

MAS NMR experiments were performed on a Bruker Avance Neo spectrometer operating at $14.09\,T$ ($600\,MHz$ ^1H Larmor frequency). A triple resonance HFX probe head from PhoenixNMR equipped with a $1.3\,mM$ MAS stator from Bruker was used with the X channel tuned to ^{13}C. Temperature calibration was done with an external $^2H_4$-methanol sample (Karschin et al. (2022)), and chemical shift referencing was done indirectly via the ^1H signal of 2,2-dimethyl-2-silapentane-5-sulfonate sodium salt (DSS). All experiments were performed at a MAS frequency of $55.555\,kHz$ and a sample temperature of approximately $309\,K$. Spectra were processed with Bruker Topspin software (versions 4.1.4 and 4.5.0).

Pulse sequence diagrams can be found in Fig. 1. All experiments were performed with ^{19}F detection ($10\,ms$ acquisition time) and ^1H and ^{13}C decoupling unless stated otherwise. Composite pulse decoupling during acquisition was typically achieved with $10\,kHz$ swfTPPM (Thakur et al. (2006)) on ^1H and $10\,kHz$ WALTZ-16 (Shaka et al. (1983)) on ^{13}C. The recycle delay was set to $\approx 1.3 * T_1$ of ^{19}F, depending on the concentration of the paramagnetic compound, except for the ^{19}F saturation recovery experiment, in which the recycle delay was set to $1.2\,s$. The pre-saturation block in the saturation recovery experiment was
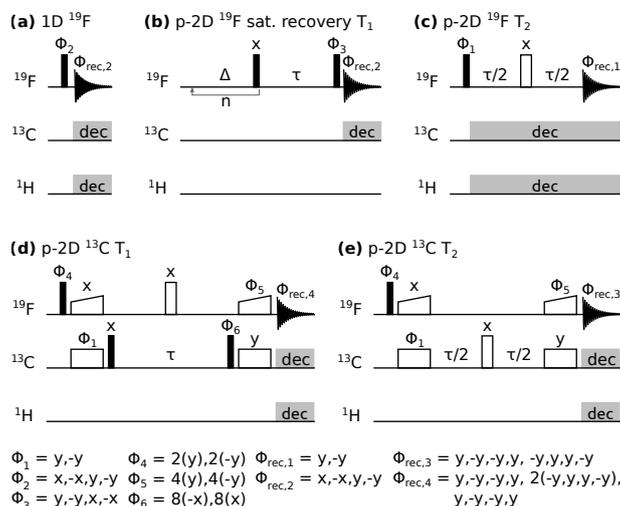
Figure 1. Puls sequences used in this study. Closed, open, and wide open rectangles denote $90°$, $180°$, and CP spin-lock pulses, respectively. Gray rectangles indicate composite pulse decoupling. Δ and τ are delays, and n indicates a loop. Puls phases are indicated above the plus with Φ_n marking a pulse undergoing phase cycling as noted below. Acquisition is denoted with a free induction decay scheme with the receiver phase $\Phi_{rec,n}$ indicated above. p-2D stands for pseudo two-dimensional spectrum with one frequency dimension and one pseudo dimension in which a delay τ is incremented.

repeated n = 50 times with a delay $\Delta = 4.5$ ms. Magnetization transfer in ^{13}C relaxation experiments was achieved via dipolar ^{19}F$-^{13}$C cross-polarization (CP) steps. Typical CP spin-lock radio-frequency field strengths were 40 kHz on ^{13}C and 90 kHz on ^{19}F with a linear ramp of 90-100% and a transfer time of 400 μs. ^{19}F and ^{13}C relaxation experiments were recorded as
125 pseudo two-dimensional spectra with one ^{19}F frequency dimension and one pseudo dimension in which a relaxation delay τ was incremented.

2.4 Relaxation rate analysis

Spectra were processed as pseudo-2D spectra in Topspin and converted to UCSF format with the bruk2ucsf program provided in Sparky (Goddard and Kneller (2008)). Python scripts for analysis of relaxation rate constants were written in-house, utilizing
130 the Nmrglue package (Helmus and Jaroniec (2013)). Spectra were split into individual 1D slices, and peaks were fitted with the routine implemented in Nmrglue. The intensities were then fitted to a mono-exponential function. Errors were determined by Monte Carlo analysis (500 iterations) using one standard deviation of the spectral noise.

3 Results and discussion

3.1 Assignment of fluorine-labeled tryptophans in TET2

135 TET2 is a dodecameric aminopeptidase from *Pyrococcus horikoshii* that has been studied extensively by MAS NMR previously (Gauto et al. (2019b, 2022). Each of the twelve identical subunits contains four tryptophan residues: W106, W136, W164, and W276 (Fig. 2a). To achieve fluorine labeling of the aromatic ring, we expressed TET2 in deuterated M9 medium and added 5-fluoroanthranilic acid, which is metabolized by the bacteria into 5-fluoro-L-tryptophan (Fig. 2b). This precursor has a $^{19}F-^{13}C$ spin pair at position 5 in the aromatic ring and is deuterated at positions 3, 4, and 6. We will refer to the labeled protein as 5FC-

140 W-TET in the remainder of this discussion. As expected, the ^{19}F MAS NMR spectrum of 5FC-W-TET shows four individual peaks (Fig. 2c, upper spectrum). For the assignment of the signals, we prepared five Trp to Phe mutants in non-deuterated medium using the commercially available precursor 5-fluoroindole (see methods section for details). The respective spectra show either one (triple mutants) or three (single mutant) signals, which allowed us to assign the four signals (Fig. 2c, bottom spectra). Note that the spectrum of the deuterated wild type is shifted due to an isotope shift (Luck et al. (1996)).

145 3.2 The effect of Gd(DTPA-BMA) and Gd(DTPA) on bulk ^{19}F and ^{13}C relaxation

In recent years, several studies have been published using biomolecular ^{19}F MAS NMR to study structural aspects of proteins (Roos et al. (2018); Duan et al. (2022); Shcherbakov et al. (2019, 2021); Porat-Dahlerbruch et al. (2022); Wang et al. (2018)). The ^{19}F T_1 relaxation time was often reported to be several seconds long, leading to a long $\tau_{r.d.}$ to obtain an optimal SNR. We measured ^{19}F T_1 of 5FC-W-TET with a saturation recovery experiment (Fig. 2d) and obtained values between $1.67 \pm 0.08\,s$

150 (W164) and $6.0 \pm 0.4\,s$ (W136). Considering the highest value, this would correspond to a recycle delay of $\tau_{r.d.} = 7.56\,s$.

To reduce the ^{19}F T_1, we used paramagnetic doping with two different Gd^{3+} chelates. We prepared samples with six concentrations of Gd(DTPA-BMA) (0, 2, 4, 6, 8, and 16 mM, Fig. 2e) and measured ^{19}F and ^{13}C T_1 and T_2 for each residue (Fig. S1, S2, S3, S4, S6). For Gd(DTPA) (Fig. 2f), we prepared samples with 2 and 8 mM of the compound and measured ^{19}F T_1 and T_2 (Fig. S5, S6). The bulk relaxation rates $R = T^{-1}$ (average over all residues) are shown in Fig. 3a-d.

155 At 8 mM Gd(DTPA), the increase of R_2 led to a broadening of the whole spectrum that made the individual peaks indistinguishable (Fig. S7). Additionally, Gd(DTPA) changed the crystallization behavior of TET2, possibly due to binding to the protein surface (Petros et al. (1990)). We therefore refrained from preparing samples with other concentrations or measuring ^{13}C relaxation rate constants.

We find that both compounds lead to an increase in R_1 as well as R_2. To quantify the effect of the two compounds, we

160 determined the longitudinal and transverse PREs (Γ_1 and Γ_2), which are given by the slope of a linear fit of the respective relaxation rate constants as a function of the concentration of paramagnetic dopant. We performed fits of the bulk and per-residue relaxation rate constants to obtain the PREs for Gd(DTPA-BMA) (^{19}F and ^{13}C; Fig. 3e-f) and for Gd(DTPA) (only ^{19}F; Fig. 3g-h).

As expected, both Γ_1 and Γ_2 are smaller for ^{13}C than for ^{19}F. This is due to the smaller gyromagnetic ratio of the carbon
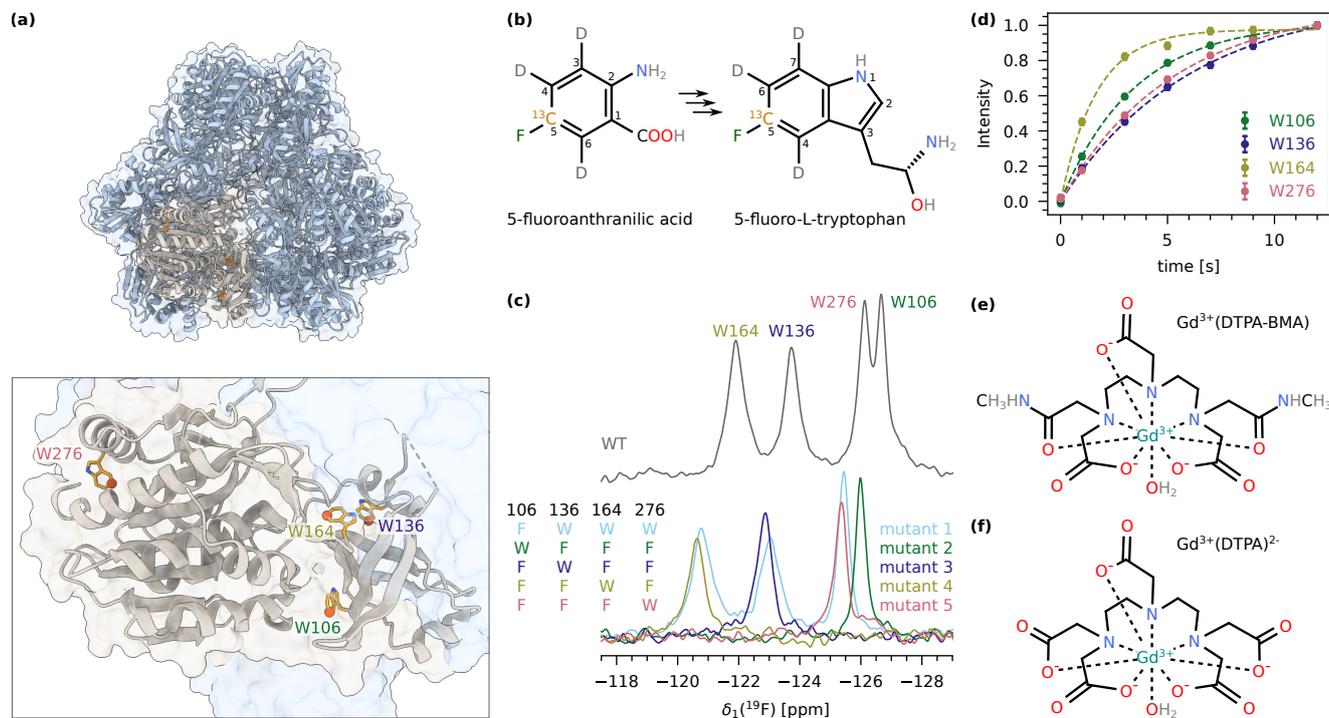
165 nucleus (Eq. (1)).

Figure 2. (a) Structure of the dodecameric TET2 (PDB: 1Y0R) (Borissenko and Groll (2005)) in cartoon representation with one subunit highlighted in beige (upper panel). The lower panel shows a close-up of one subunit with the four tryptophans indicated as orange sticks. Position 5 in the tryptophan ring is highlighted with spheres. (b) Structure of 5-fluoroanthranilic acid (left), which is converted into 5-fluoro-L-tryptophan (right) by the bacteria. (c) 1D ^{19}F MAS NMR spectrum of 5FC-W-TET. The upper panel displays the spectrum of the wild type, showing all four tryptophan peaks. The lower panel shows spectra of the five assignment mutants (mutant 1: W106F; mutant 2: W136F, W164F, W276F; mutant 3: W106F, W164F, W276F; mutant 4: W106F, W136F, W276F; mutant 5: W106F, W136F, W164F; see methods section for details). The resulting assignment is indicated at the top. The wild-type spectrum is shifted due to the isotope shift, as this sample is deuterated compared to the mutants. (d) Exponential fits of ^{19}F saturation recovery experiments on 5FC-W-TET without paramagnetic dopant. (e) Structure of Gd(DTPA-BMA). (f) Structure of Gd(DTPA).

Interestingly, the measured ^{19}F PREs for Gd(DTPA) are much higher than for Gd(DTPA-BMA). The bulk effect of Gd(DTPA) on R_1 ($\Gamma_1 = 0.743 \pm 0.015\,\text{s}^{-1}\,\text{mM}^{-1}$) is roughly seven times stronger than the effect of Gd(DTPA-BMA) ($\Gamma_1 = 0.101 \pm 0.028\,\text{s}^{-1}\,\text{mM}^{-1}$). For Γ_2, the difference is even bigger: The bulk value for Gd(DTPA) ($\Gamma_2 = 556.2 \pm 0.7\,\text{s}^{-1}\,\text{mM}^{-1}$) is over 14 times higher than the value for Gd(DTPA-BMA) ($\Gamma_2 = 38.2 \pm 0.6\,\text{s}^{-1}\,\text{mM}^{-1}$). The differences in relaxation behavior are likely the result of the specific physicochemical properties of the two compounds, such as the slower water exchange rate of Gd(DTPA-BMA) (Caravan et al. (1999)).

We find that in our case, paramagnetic doping with $8\,\text{mM}$ Gd(DTPA-BMA) is the best compromise between a significant reduction of ^{19}F T_1 without heavily compromising T_2 and therefore spectral resolution. The decrease in bulk T_1 from $3.2 \pm 1.3\,\text{s}$ at $0\,\text{mM}$ to $0.92 \pm 0.25\,\text{s}$ at $8\,\text{mM}$ Gd(DTPA-BMA) translates to a reduction of $\tau_{\text{r.d.}}$ from $4.0 \pm 1.6\,\text{s}$ to $1.2 \pm 0.4\,\text{s}$. The more
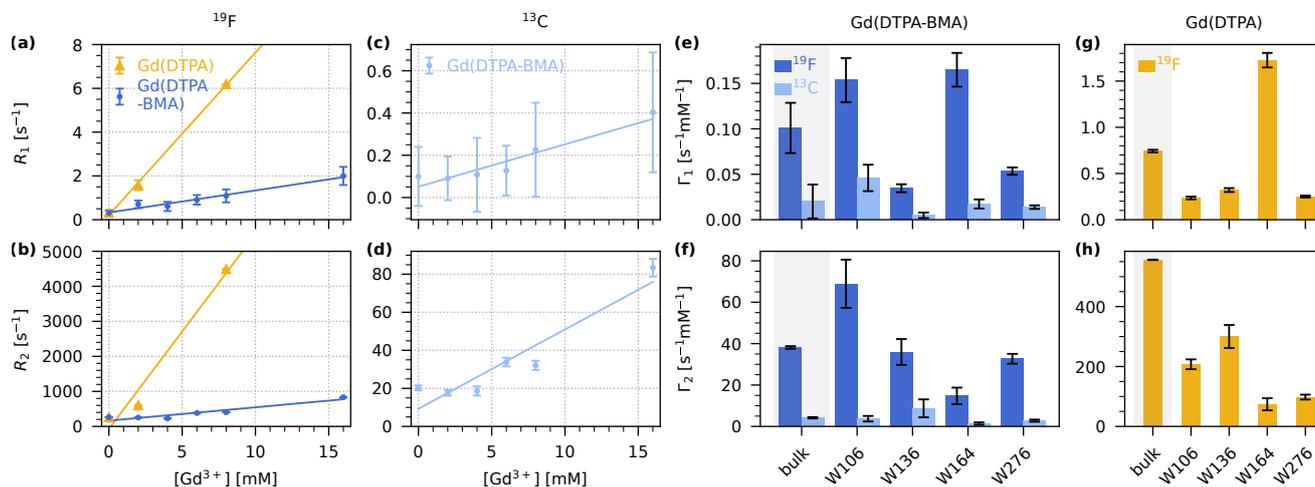
Figure 3. ^{19}F and ^{13}C longitudinal and transverse PRE (Γ_1 and Γ_2) for Gd(DTPA-BMA) and Gd(DTPA) measured on 5FC-W-Trp. (a-b) Linear fits of bulk ^{19}F R_1 (a) and R_2 (b) relaxation rate constants as a function of the concentration of Gd(DTPA-BMA) (blue) and Gd(DTPA) (yellow). (c-d) Linear fits of bulk ^{13}C R_1 (c) and R_2 (d) relaxation rate constants as a function of the concentration of Gd(DTPA-BMA) (light blue). (e) ^{19}F (dark blue) and ^{13}C (light blue) Γ_1 (e) and Γ_2 (f) for Gd(DTPA-BMA). (g) ^{19}F Γ_1 (g) and Γ_2 (h) for Gd(DTPA). The bulk relaxation rate constants in (a-d) are the average over the four residues (see Fig. S1, S2, S3, S4, S5) except for the rate at 8 mM Gd(DTPA), which was only measured as a bulk rate due to line broadening. In (e-h), the first bar of each plot is the bulk PRE resulting from the fits in (a-d) (gray background), followed by the individual values for each residue resulting from the fits in Fig. S1, S2, S3, S4, S5. Note that the per-residue fits for Gd(DTPA) (g,h) are performed with only two points (0 and 2 mM) while the bulk fit is performed with three points (0, 2, and 8 mM). This leads to a deviation between Γ^{bulk} and the average over the residue-wise values.

175 than 3-fold shorter recycle delay significantly reduces the measurement times of ^{19}F MAS NMR spectra, or, in other words, increases the SNR per unit time. Although the same effect could be achieved with lower concentrations of Gd(DTPA), we prefer the use of Gd(DTPA-BMA) due to a potential interaction of Gd(DTPA) with the protein in our case (see above).

3.3 The relative PREs of individual tryptophan residues

The observed PREs for the individual tryptophans differ (Fig. 3e-h), which can be expected as they are impacted by a multitude
180 of factors, such as the solvent accessibility of the residue, its dynamics, or the density of surrounding protons (Tang et al. (2011); Wickramasinghe et al. (2009)). The influences of these factors can conversely even be used to characterize the surfaces and interaction interfaces of proteins with so-called solvent PREs (Pintacuda and Otting (2002); Öster et al. (2017); Hocking et al. (2013)).

To rationalize the observed PRE data for the four Trp sites, we compared them to structural parameters. We reasoned that
185 the relaxation properties may be impacted by the ^{1}H spins surrounding each of the ^{19}F Trp sites, and calculated the root-sum-square dipolar coupling d^{rss} (Fig. S8a). This parameter approximates the effective dipolar-coupling network and can serve as an indicator for spin diffusion, which influences the propagation of the PRE effect throughout the protein. It was calculated as the

square root of the sum of squared dipolar couplings between a fluorine and all back-exchangeable protons (Zorin et al. (2006)). Moreover, we calculated the solvent accessible surface area (SASA) of each tryptophan (Fig. S8b), which is an approximate

190   measure of the shortest distance between the paramagnetic compound and a given ^{19}F atom. In our case, we did not find a direct correlation of these parameters with the observed PREs (Fig. S8c-d).

Interestingly, the PRE patterns (relative strength of the measured PREs for the four residues) are different for different relaxation rate constants (Γ_1 and Γ_2), different compounds, and different nuclei (^{19}F and ^{13}C)(Fig. 3e-h). In addition to the factors mentioned above, other influencing parameters that could explain these different patterns include a lower spin diffusion

195   efficiency for ^{13}C, specific binding of the Gd^{3+} complex to the protein, and properties of the compound, such as the rotational correlation time τ_c or the water exchange rate.

Differences between the patterns observed for Gd(DTPA-BMA) and Gd(DTPA) could be due to the specific binding of one of the complexes to the protein. A decrease in the distance r between the compound and residues close to the binding site would increase the observed PRE effects as both Γ_1 and Γ_2 are proportional to r^{-6} (Eq. (1)). The binding would also decrease

200   τ_c of the compound, which could, in combination with the dynamics of a specific tryptophan, lead to dampening or acceleration of the PRE.

The most striking observation is that the ^{19}F Γ^1 of W164 is very high relative to the other residues compared to ^{19}F Γ^2 for both Gd^{3+} complexes. Such a difference between the longitudinal and transverse PRE can also be a result of a local reduction of τ_c due to binding. As Γ_1 and Γ_2 sample the spectral density at different frequencies, their reaction to changes of τ_c is not the

205   same (Eq. (1)) (Jaroniec (2012)). The complex interplay of diverse parameters makes it difficult to understand these patterns in detail.

4   Conclusions

The potential of biomolecular ^{19}F MAS NMR is often limited by long T_1 relaxation times that require recycle delays of several seconds. In this work, we discussed the application of paramagnetic doping with Gd^{3+} complexes to accelerate these

210   experiments. Previously, paramagnetic doping with different compounds was used to reduce the ^{1}H T_1 in a variety of sample types, such as membrane proteins and protein microcrystals (Wickramasinghe et al. (2007, 2009); Linser et al. (2007); Ullrich et al. (2014)). To our knowledge, this is the first study applying paramagnetic doping for MAS NMR to fluorine-labeled biological samples.

We evaluated the effect of two different Gd^{3+} complexes, Gd(DTPA-BMA) and Gd(DTPA), on the ^{19}F and ^{13}C T_1 and T_2

215   relaxation times in deuterated and 5-fluorotryptophan-labeled TET2. The addition of $8\,\mathrm{mM}$ Gd(DTPA-BMA) reduces $\tau_{\mathrm{r.d.}}$ by a factor of more than 3 compared to the undoped sample without causing significant line broadening. The addition of Gd(DTPA) results in a stronger paramagnetic relaxation enhancement, but it is a less favourable compound due to its interaction with the protein.

We anticipate that the use of paramagnetic doping for biomolecular ^{19}F MAS NMR can be applied to a variety of systems,

220   experiments, and different types of sample preparations. The increase in sensitivity will be especially beneficial for structural

studies and the measurement of anisotropic spin interactions. As for paramagnetic doping of non-fluorine-labeled samples, the optimal concentration and compound are likely to depend on the specific experimental setup.

Code and data availability. NMR spectra, analysis scripts, and raw data are publicly available at the ISTA research explorer (DOI: 10.15479/AT-ISTA-21284) (Becker and Schanda (2026)).

225 *Author contributions.* P.S. and L.M.B. designed the project. G.T. synthesized the 5FC-anthranilic acid. A.K., R.S., and U.G. prepared proteins. L.M.B. prepared samples, performed solid-state NMR experiments, analyzed data, and prepared figures. L.M.B., P.S., and G.T. wrote the manuscript. All authors discussed and commented on the manuscript.

Competing interests. At least one of the (co-)authors is a member of the editorial board of Magnetic Resonance.

MAGNETIC RESONANCE
Open Access Discussions

References

235   Becker, L. M. and Schanda, P.: Research data for 'Accelerated 19F biomolecular magic-angle spinning NMR with paramagnetic dopants', https://doi.org/10.15479/AT-ISTA-21284, 2026.

Bertini, I., Luchinat, C., and Giacomo, P., eds.: Solution NMR of Paramagnetic Molecules: Applications to Metallobiomolecules and Models, vol. 2 of *Curr. Methods Inorg. Chem.*, Elsevier, 2001.

Bloembergen, N. and Morgan, L. O.: Proton relaxation times in paramagnetic solutions. Effects of electron spin relaxation, J. Chem. Phys.,
240   34, 842–850, https://doi.org/10.1063/1.1731684, 1961.

Boeszoermenyi, A., Chhabra, S., Dubey, A., Radeva, D. L., Burdzhiev, N. T., Chanev, C. D., Petrov, O. I., Gelev, V. M., Zhang, M., Anklin, C., Kovacs, H., Wagner, G., Kuprov, I., Takeuchi, K., and Arthanari, H.: Aromatic ^{19}F-^{13}C TROSY: a background-free approach to probe biomolecular structure, function, and dynamics, Nat. Methods, 16, 333–340, https://doi.org/10.1038/s41592-019-0334-x, 2019.

Bondarenko, V., Wells, M. M., Chen, Q., Singewald, K. C., Saxena, S., Xu, Y., and Tang, P.: ^{19}F Paramagnetic Relaxation-Based NMR for
245   Quaternary Structural Restraints of Ion Channels, ACS Chem. Biol., 14, 2160–2165, https://doi.org/10.1021/acschembio.9b00692, 2019.

Borissenko, L. and Groll, M.: Crystal structure of TET protease reveals complementary protein degradation pathways in prokaryotes, J. Mol. Biol., 346, 1207–1219, https://doi.org/10.1016/j.jmb.2004.12.056, 2005.

Caravan, P., Ellison, J. J., McMurry, T. J., and Lauffer, R. B.: Gadolinium(III) chelates as MRI contrast agents: Structure, dynamics, and applications, Chem. Rev., 99, 2293–2352, https://doi.org/10.1021/cr980440x, 1999.

250   Duan, P., Dregni, A. J., and Hong, M.: Solid-State NMR ^{19}F-^{1}H-^{15}N Correlation Experiments for Resonance Assignment and Distance Measurements of Multifluorinated Proteins, J. Phys. Chem. A, 126, 7021–7032, https://doi.org/10.1021/acs.jpca.2c05154, 2022.

Gauto, D. F., Estrozi, L. F., Schwieters, C. D., Effantin, G., Macek, P., Sounier, R., Sivertsen, A. C., Schmidt, E., Kerfah, R., Mas, G., Colletier, J. P., Güntert, P., Favier, A., Schoehn, G., Schanda, P., and Boisbouvier, J.: Integrated NMR and cryo-EM atomic-resolution structure determination of a half-megadalton enzyme complex, Nat. Commun., 10, 2697, https://doi.org/10.1038/s41467-019-10490-9,
255   2019a.

Gauto, D. F., Macek, P., Barducci, A., Fraga, H., Hessel, A., Terauchi, T., Gajan, D., Miyanoiri, Y., Boisbouvier, J., Lichtenecker, R., Kainosho, M., and Schanda, P.: Aromatic Ring Dynamics, Thermal Activation, and Transient Conformations of a 468 kDa Enzyme by Specific ^{1}H-^{13}C Labeling and Fast Magic-Angle Spinning NMR, J. Am. Chem. Soc., 141, 11 183–11 195, https://doi.org/10.1021/jacs.9b04219, 2019b.

260   Gauto, D. F., Macek, P., Malinverni, D., Fraga, H., Paloni, M., Sučec, I., Hessel, A., Bustamante, J. P., Barducci, A., and Schanda, P.: Functional control of a 0.5 MDa TET aminopeptidase by a flexible loop revealed by MAS NMR, Nature Communications, 13, 1927, https://doi.org/10.1038/s41467-022-29423-0, 2022.

Goddard, T. D. and Kneller, D. G.: SPARKY 3, University of California, San Francisco, 2008.

Gronenborn, A. M.: Small, but powerful and attractive: ^{19}F in biomolecular NMR, https://doi.org/10.1016/j.str.2021.09.009, 2022.

265   Heller, G. T., Shukla, V. K., Figueiredo, A. M., and Hansen, D. F.: Picosecond Dynamics of a Small Molecule in Its Bound State with an Intrinsically Disordered Protein, J. Am. Chem. Soc., 146, 2319–2324, https://doi.org/10.1021/jacs.3c11614, 2024.

Helmus, J. J. and Jaroniec, C. P.: Nmrglue: An open source Python package for the analysis of multidimensional NMR data, J. Biomol. NMR, 55, 355–367, https://doi.org/10.1007/s10858-013-9718-x, 2013.

Hocking, H. G., Zangger, K., and Madl, T.: Studying the structure and dynamics of biomolecules by using soluble paramagnetic probes,
270   ChemPhysChem, 14, 3082–3094, https://doi.org/10.1002/cphc.201300219, 2013.

Huang, Y., Wang, X., Lv, G., Razavi, A. M., Huysmans, G. H., Weinstein, H., Bracken, C., Eliezer, D., and Boudker, O.: Use of paramagnetic ^{19}F NMR to monitor domain movement in a glutamate transporter homolog, Nat. Chem. Biol., 16, 1006–1012, https://doi.org/10.1038/s41589-020-0561-6, 2020.

Jaroniec, C. P.: Solid-state nuclear magnetic resonance structural studies of proteins using paramagnetic probes, https://doi.org/10.1016/j.ssnmr.2012.02.007, 2012.

Juen, F., Glänzer, D., Plangger, R., Kugler, V., Fleischmann, J., Stefan, E., Case, D. A., Kovacs, H., Dayie, T. K., and Kreutz, C.: Enhanced TROSY Effect in [2-^{19}F, 2-^{13}C] Adenosine and ATP Analogs Facilitates NMR Spectroscopy of Very Large Biological RNAs in Solution, Angew. Chem. Int. Ed., 63, e202316 273, https://doi.org/10.1002/anie.202316273, 2024.

Karschin, N., Krenek, S., Heyer, D., and Griesinger, C.: Extension and improvement of the methanol-d4 NMR thermometer calibration, Magn. Reson. Chem., 60, 203–209, https://doi.org/10.1002/mrc.5216, 2022.

Konig, S. H.: A classical description of relaxation of interacting pairs of unlike spins: Extension to $T_{1\rho}$, T_2, and $T_{1\rho off}$, including contact interactions, J. Magn. Reson. (1969), 47, 441–453, https://doi.org/10.1016/0022-2364(82)90211-6, 1982.

Linser, R., Chevelkov, V., Diehl, A., and Reif, B.: Sensitivity enhancement using paramagnetic relaxation in MAS solid-state NMR of perdeuterated proteins, J. Magn. Reson., 189, 209–216, https://doi.org/10.1016/j.jmr.2007.09.007, 2007.

Lu, X., Lu, X., Tsutsumi, Y., Huang, C., Xu, W., Byrn, S. R., Templeton, A. C., Buevich, A. V., Amoureux, J. P., Amoureux, J. P., Amoureux, J. P., Su, Y., Su, Y., and Su, Y.: Molecular packing of pharmaceuticals analyzed with paramagnetic relaxation enhancement and ultrafast magic angle pinning NMR, Phys. Chem. Chem. Phys.s, 22, 13 160–13 170, https://doi.org/10.1039/d0cp02049d, 2020.

Luck, L. A., Vance, J. E., O'Connell, T. M., and London, R. E.: ^{19}F NMR relaxation studies on 5-fluorotryptophan- and tetradeutero-5-fluorotryptophan-labeled E. coli Glucose/Galactose Receptor, JJ. Biomol. NMR, 7, 261–272, https://doi.org/10.1007/BF00200428, 1996.

Matei, E. and Gronenborn, A. M.: ^{19}F Paramagnetic Relaxation Enhancement: A Valuable Tool for Distance Measurements in Proteins, Angew. Chem. Int. Ed., 55, 150–154, https://doi.org/10.1002/anie.201508464, 2016.

Mroue, K. H., Zhang, R., Zhu, P., McNerny, E., Kohn, D. H., Morris, M. D., and Ramamoorthy, A.: Acceleration of natural-abundance solid-state MAS NMR measurements on bone by paramagnetic relaxation from gadolinium-DTPA, J. Magn. Reson., 244, 90–97, https://doi.org/10.1016/j.jmr.2014.04.020, 2014.

Öster, C., Kosol, S., Hartlmüller, C., Lamley, J. M., Iuga, D., Oss, A., Org, M. L., Vanatalu, K., Samoson, A., Madl, T., and Lewandowski, J. R.: Characterization of Protein-Protein Interfaces in Large Complexes by Solid-State NMR Solvent Paramagnetic Relaxation Enhancements, J. Am. Chem. Soc., 139, 12 165–12 174, https://doi.org/10.1021/jacs.7b03875, 2017.

Öster, C., Kosol, S., and Lewandowski, J. R.: Quantifying Microsecond Exchange in Large Protein Complexes with Accelerated Relaxation Dispersion Experiments in the Solid State, Sci. Rep., 9, 11 082, https://doi.org/10.1038/s41598-019-47507-8, 2019.

Overbeck, J. H., Kremer, W., and Sprangers, R.: A suite of ^{19}F based relaxation dispersion experiments to assess biomolecular motions, J. Biomol. NMR, 74, 753–766, https://doi.org/10.1007/s10858-020-00348-4, 2020.

Petros, A. M., Mueller, L., and Kopple, K. D.: NMR Identification of Protein Surfaces Using Paramagnetic Probes, Biochemistry, 29, 10 041–10 048, https://doi.org/10.1021/bi00495a005, 1990.

Pintacuda, G. and Otting, G.: Identification of protein surfaces by NMR measurements with a paramagnetic Gd(III) chelate, J. Am. Chem. Soc., 124, 372–373, https://doi.org/10.1021/ja016985h, 2002.

Porat-Dahlerbruch, G., Struppe, J., Quinn, C. M., Gronenborn, A. M., and Polenova, T.: Determination of accurate ^{19}F chemical shift tensors with R-symmetry recoupling at high MAS frequencies (60–100 kHz), J. Magn. Reson., 340, 107 227, https://doi.org/10.1016/j.jmr.2022.107227, 2022.

Roos, M., Wang, T., Shcherbakov, A. A., and Hong, M.: Fast Magic-Angle-Spinning ^{19}F Spin Exchange NMR for Determining Nanometer [19]F-[19]F Distances in Proteins and Pharmaceutical Compounds, J. Phys. Chem. B, 122, 2900–2911, https://doi.org/10.1021/acs.jpcb.8b00310, 2018.

Schanda, P.: Fast-pulsing longitudinal relaxation optimized techniques: Enriching the toolbox of fast biomolecular NMR spectroscopy, Progr. Nucl. Magn. Reson. Spectrosc., 55, 238–265, https://doi.org/10.1016/j.pnmrs.2009.05.002, 2009.

Sengupta, I.: Insights into the Structure and Dynamics of Proteins from ^{19}F Solution NMR Spectroscopy, https://doi.org/10.1021/acs.biochem.4c00534, 2024.

Shaka, A. J., Keeler, J., Frenkiel, T., and Freeman, R.: An improved sequence for broadband decoupling: WALTZ-16, J. Magn. Reson. (1969), 52, 335–338, https://doi.org/10.1016/0022-2364(83)90207-X, 1983.

Shcherbakov, A. A., Mandala, V. S., and Hong, M.: High-Sensitivity Detection of Nanometer [1]H-[19]F Distances for Protein Structure Determination by ^{1}H-Detected Fast MAS NMR, J. Phys. Chem. B, 123, 4387–4391, https://doi.org/10.1021/acs.jpcb.9b03812, 2019.

Shcherbakov, A. A., Hisao, G., Mandala, V. S., Thomas, N. E., Soltani, M., Salter, E. A., Davis, J. H., Henzler-Wildman, K. A., and Hong, M.: Structure and dynamics of the drug-bound bacterial transporter EmrE in lipid bilayers, Nat. Commun., 12, 1–13, https://doi.org/10.1038/s41467-020-20468-7, 2021.

Shi, P., Li, D., Li, J., Chen, H., Wu, F., Xiong, Y., and Tian, C.: Application of site-specific ^{19}F paramagnetic relaxation enhancement to distinguish two different conformations of a multidomain protein, J. Phys. Chem. Lett., 3, 34–37, https://doi.org/10.1021/jz201480g, 2012.

Solomon, I.: Relaxation processes in a system of two spins, Phys. Rev., 99, 559–565, https://doi.org/10.1103/PhysRev.99.559, 1955.

Suleiman, M., Frere, G. A., Törner, R., Tabunar, L., Bhole, G. V., Taverner, K., Tsuchimura, N., Pichugin, D., Lichtenecker, R. J., Vozny, O., Gunning, P., Arthanari, H., Sljoka, A., and Prosser, R. S.: Characterization of conformational states of the homodimeric enzyme fluoroacetate dehalogenase by ^{19}F-^{13}C two-dimensional NMR, RSC Chem. Biol., 5, 1214–1218, https://doi.org/10.1039/d4cb00176a, 2024.

Tang, M., Berthold, D. A., and Rienstra, C. M.: Solid-state NMR of a large membrane protein by paramagnetic relaxation enhancement, J. Phys. Chem. Lett., 2, 1836–1841, https://doi.org/10.1021/jz200768r, 2011.

Thakur, R. S., Kurur, N. D., and Madhu, P. K.: Swept-frequency two-pulse phase modulation for heteronuclear dipolar decoupling in solid-state NMR, Chem. Phys. Lett., 426, 459–4, https://doi.org/10.1016/j.cplett.2006.06.007, 2006.

Toscano, G., Holzinger, J., Nagl, B., Kontaxis, G., Kählig, H., Konrat, R., and Lichtenecker, R. J.: Decorating phenylalanine side-chains with triple labeled ^{13}C/^{19}F/^{2}H isotope patterns, J. Biomol. NMR, 78, 139–147, https://doi.org/10.1007/s10858-024-00440-z, 2024a.

Toscano, G., Rosati, M., Barbieri, L., Maier, K., Banci, L., Luchinat, E., Konrat, R., and Lichtenecker, R. J.: The synthesis of specifically isotope labelled fluorotryptophan and its use in mammalian cell-based protein expression for ^{19}F-NMR applications, Chem. Commun., 60, 14 188–14 191, https://doi.org/10.1039/d4cc04789c, 2024b.

Ullrich, S. J., Hölper, S., and Glaubitz, C.: Paramagnetic doping of a 7TM membrane protein in lipid bilayers by Gd 3+-complexes for solid-state NMR spectroscopy, J. Biomol. NMR, 58, 27–35, https://doi.org/10.1007/s10858-013-9800-4, 2014.

Ulrich, A. S.: Solid state ^{19}F NMR methods for studying biomembranes, https://doi.org/10.1016/j.pnmrs.2004.11.001, 2005.

Wang, M., Lu, M., Fritz, M. P., Quinn, C. M., Byeon, I. J. L., Byeon, C. H., Struppe, J., Maas, W., Gronenborn, A. M., and Polenova, T.: Fast Magic-Angle Spinning ^{19}F NMR Spectroscopy of HIV-1 Capsid Protein Assemblies, Angew. Chem. Int. Ed., 57, 16 375–16 379, https://doi.org/10.1002/anie.201809060, 2018.

345 Wickramasinghe, N. P., Kotecha, M., Samoson, A., Past, J., and Ishii, Y.: Sensitivity enhancement in ^{13}C solid-state NMR of protein microcrystals by use of paramagnetic metal ions for optimizing ^{1}H T_1 relaxation, J. Magn. Reson., 184, 350–356, https://doi.org/10.1016/j.jmr.2006.10.012, 2007.

Wickramasinghe, N. P., Parthasarathy, S., Jones, C. R., Bhardwaj, C., Long, F., Kotecha, M., Mehboob, S., Fung, L. W., Past, J., Samoson, A., and Ishii, Y.: Nanomole-scale protein solid-state NMR by breaking intrinsic ^{1}H T_1 boundaries, Nat. Methods, 6, 215–218,
350   https://doi.org/10.1038/nmeth.1300, 2009.

Zorin, V. E., Brown, S. P., and Hodgkinson, P.: Quantification of homonuclear dipolar coupling networks from magic-angle spinning ^{1}H NMR, Molecular Physics, 104, 293–304, https://doi.org/10.1080/00268970500351052, 2006.